

Analytical solutions for buckling of simply supported rectangular plates due to non-linearly distributed in-plane bending stresses

Prasun Jana[†] and K. Bhaskar[‡]

Aerospace Engineering Department, IIT, Madras, Chennai – 600 036, India

(Received December 20, 2005, Accepted November 10, 2006)

Abstract. Rigorous analytical solutions are obtained for the plane stress problem of a rectangular plate subjected to non-linearly distributed bending loads on two opposite edges. They are then used in a Galerkin type solution to obtain the corresponding convergent buckling loads. It is shown that the critical bending moment depends significantly on the actual edge load distribution and further the number of nodal lines of the buckled configuration can also be different from that corresponding to a linear antisymmetric distribution of the bending stresses. Results are tabulated for future use while judging approximate numerical solutions.

Keywords: buckling; rectangular plates; in-plane bending; non-linear edge stress distribution; two-dimensional elasticity; analytical solutions.

1. Introduction

Plate problems are often idealisations of portions of a much more complicated stiffened or built-up structure, for example, a rectangular portion of an aircraft wing skin bounded by orthogonal stiffeners or the web of a box girder. Instead of analyzing this overall structure, one attempts to isolate the small portion of interest and analyze it separately, for the sake of simplicity, using plate theory. However, while doing so one has to keep in mind that the boundary conditions and the loads can then be specified only intuitively because they depend on the relative stiffnesses of the separated free bodies. In addition to the analysis of this intuitive problem, it is thus necessary to find out the effect of a possible change in boundary conditions or load distribution.

Based on this reasoning, and with specific reference to the problem of stability of rectangular plates, it is necessary to obtain results for different boundary conditions and statically equivalent load distributions. While the classical problems of uniform uniaxial and biaxial compression and in-plane shear have been extensively studied for plates with different boundary conditions (Timoshenko and Gere 1961), non-uniform variations of loading have also been considered. Some notable early investigations in this regard have been those of Timoshenko (1910) for collinear concentrated loads by means of an energy method which does not require the complete

[†] Research Scholar

[‡] Professor, Corresponding author, E-mail: kbhas@ae.iitm.ac.in

determination of the in-plane stress field, and Benoy (1969) for a parabolically distributed load using an assumed in-plane stress distribution. More recently, Leissa and Ayoub (1988) considered the case of collinear concentrated loads using a combination of finite element method for plane stress analysis and Ritz method for stability analysis. Similarly, stiffened plates under partial edge loading were studied using finite element method by Srivastava *et al.* (2003). As an alternative to finite element method, the use of mesh free method has been advocated by Liew and Chen (2004) and Chen and Liew (2004) who considered moderately thick/functionally graded plates under non-uniform loading. The influence of non-uniform loading on laterally restrained plates was examined by Bedair (1996). Orthotropic plates under parabolic loading have been studied by Hu *et al.* (2003) using an assumed plane stress field. Bert and Devarakonda (2003) studied plates under sinusoidally distributed load and showed that it is necessary to carry out the plane stress analysis carefully to obtain correct values of the buckling load. Very recently, a comprehensive set of rigorous analytical solutions have been obtained for a simply supported plate subjected to various uniaxial stress distributions (Jana and Bhaskar 2004, Jana 2005) and it has been shown that the total buckling load of a square plate can vary significantly (between 65% to 166%) from that corresponding to uniform stress distribution.

All the above-mentioned investigations are with reference to uniaxial compression. With reference to the related problem of buckling due to uniaxial in-plane bending loads, a number of investigators have studied the effect of a linear antisymmetric bending stress distribution. For example, the classical text-book of Bulson (1970) cites and presents results, based on approximate energy methods, for various combinations of classical and non-classical boundary conditions on the loaded ends and the longitudinal sides. Recently Leissa and Kang (2002) adopted a Frobenius' series approach and obtained an exact solution for the specific case of a plate with simply supported loaded ends and clamped sides, with the load varying linearly along the loaded ends; they later extended it to arbitrary boundary conditions on the unloaded sides (Kang and Leissa 2005).

From the above literature survey, it is clear that the practically important problem of plate buckling due to non-uniform loading has been the focus of many recent studies but almost all of them have been confined to loads causing uniaxial compression. The present work aims to expand this knowledge base by considering the effect of non-linear bending stress distributions. While the general remarks made earlier justify such a study, it is also appropriate in the light of observations with reference to the effects of transverse shear deformation in not-so-slender beams. For example, the plane stress solution corresponding to a simply supported beam (Little 1973), shows that the bending stress does not vary linearly but in a complex nonlinear fashion which approaches the linear distribution asymptotically as the beam becomes longer and longer. Thus, when a relatively short box beam undergoes bending, the webs are subjected to nonlinearly distributed bending stresses. Similarly, with reference to the sheet stiffener combination that is typical of aircraft construction, the actual service loads are usually transmitted to the skin through the stiffeners, and thus any in-plane bending action on a rectangular portion of the skin is basically due to localized forces at the ends of opposite sides.

The present study is based on a rigorous superposition methodology for plane stress analysis and a Galerkin type solution with a set of complete admissible functions for stability analysis. Attention is confined to plates simply supported all around and the effect of five different uniaxial bending stress distributions on the overall value of the critical moment is examined.

2. Plane stress analysis

The different antisymmetric bending stress distributions, applied on the edges $x = \pm a/2$, are as shown in Fig. 1. They are listed in an order such that the moment arm between the resultants of the tensile and compressive stresses increases. Each of the load cases of Fig. 1 can be analyzed rigorously by using a superposition of three Airy's stress functions (or building blocks), taken in the form of appropriate single Fourier series (Little 1973) as described below.

All the cases except load case 1 (full sine load) can be divided into two parts where the first part

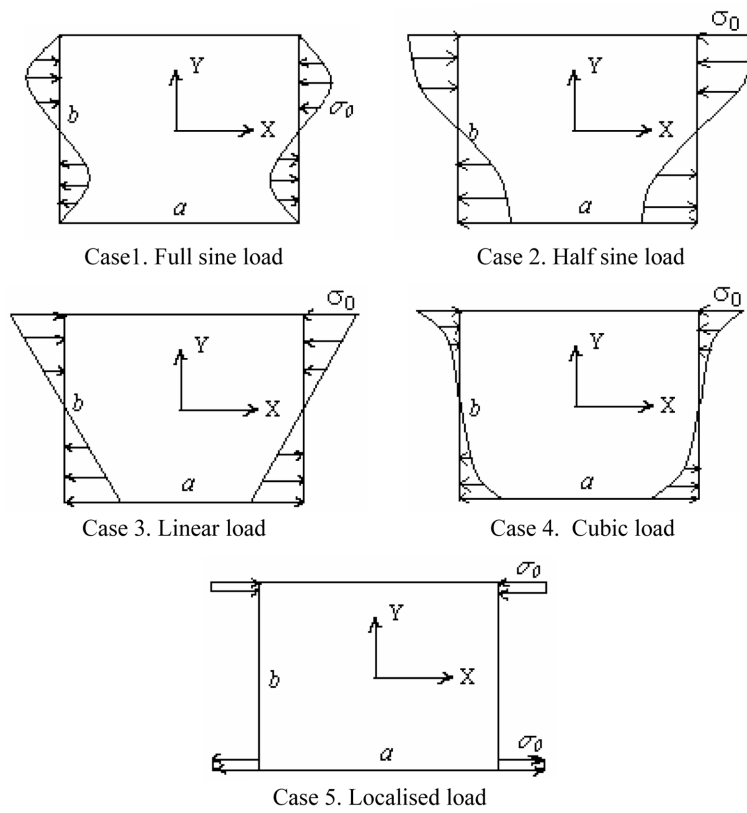


Fig. 1 Various load cases considered

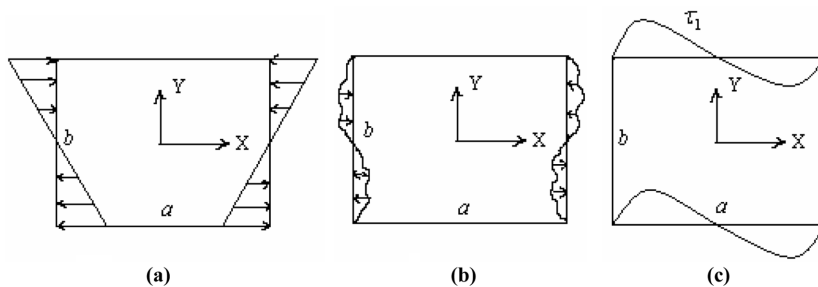


Fig. 2 (a) The linear antisymmetric component, (b) The nonlinear component – Building block 1, (c) The corresponding residual shear stress

(Fig. 2(a)) is one for which the in-plane stress distribution is linear everywhere in the domain of the plate. It is necessary to find out the plane stress solution only for the remaining part (Fig. 2(b)) and this is in terms of the following building blocks. Load case 1 directly corresponds to the second part.

2.1 Building block 1

The appropriate series representation of the normal stress of Fig. 2(b) is taken as

$$\sigma_x = \sum_{r=2,4,6..} \sigma_r \sin\left(\frac{r\pi y}{b}\right) \quad (1)$$

Substituting the Airy stress function ϕ_1 given by

$$\phi_1 = \sum_{r=2,4,6..} f(x) \sin\left(\frac{r\pi y}{b}\right) \quad (2)$$

into the governing biharmonic equation $\nabla^4 \phi = 0$, one can obtain the general solution for the function $f(x)$ as

$$f(x) = \sum_{r=2,4,6..} C_{1r} \cosh\left(\frac{r\pi x}{b}\right) + C_{2r} \sinh\left(\frac{r\pi x}{b}\right) + C_{3r} x \cosh\left(\frac{r\pi x}{b}\right) + C_{4r} x \sinh\left(\frac{r\pi x}{b}\right) \quad (3)$$

in which C_{1r} through C_{4r} are constants which are to be obtained from the boundary conditions.

It has to be noted that this stress function solution automatically gives a zero normal stress at $y = \pm b/2$. Enforcement of the zero shear stress boundary condition as well as the normal stress distribution as defined in Eq. (1) at $x = \pm a/2$, yields

$$\phi_1 = \sum_{r=2,4,6..} \sin\left(\frac{r\pi y}{b}\right) \left[C_{1r} \cosh\left(\frac{r\pi x}{b}\right) + C_{4r} x \sinh\left(\frac{r\pi x}{b}\right) \right] \quad (4)$$

where C_{1r} and C_{4r} are given by

$$C_{1r} = -\frac{b^2 \sigma_r \left[ar\pi \cosh\left(\frac{ar\pi}{2b}\right) + 2b \sinh\left(\frac{ar\pi}{2b}\right) \right]}{r^2 \pi^2 \left[ar\pi + b \sinh\left(\frac{ar\pi}{b}\right) \right]} \quad \text{and} \quad C_{4r} = \frac{2b^2 \sigma_r \sinh\left(\frac{ar\pi}{2b}\right)}{ar^2 \pi^2 + br\pi \sinh\left(\frac{ar\pi}{b}\right)} \quad (5)$$

But this produces a residual shear stress (Fig. 2(c)) at $y = \pm b/2$ as

$$\tau_1 = - \sum_{r=2,4,6..} \frac{r\pi}{b} \cos\left(\frac{r\pi}{2}\right) \left[\left(C_{1r} \frac{r\pi}{b} + C_{4r} \right) \sinh\left(\frac{r\pi x}{b}\right) + C_{4r} \frac{r\pi}{b} x \cosh\left(\frac{r\pi x}{b}\right) \right] \quad (6)$$

which is neutralized by the next two building blocks.

2.2 Building block 2

The second building block, is due to shear stresses applied at $y = \pm b/2$ and represented by the

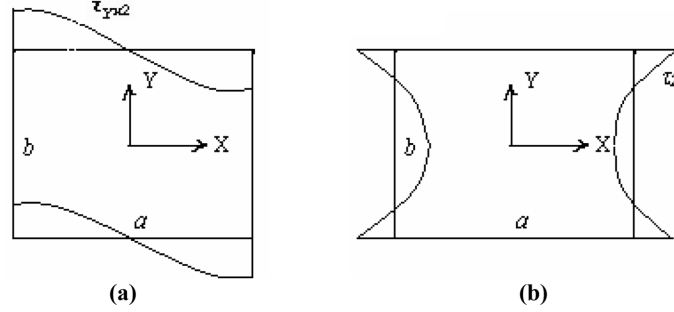


Fig. 3 (a) Building block 2, (b) The corresponding residual shear stress

Fourier sine series

$$\tau_{yx2} = \sum_{m=1,3,5} A_m \sin\left(\frac{m\pi x}{a}\right) \quad (7)$$

with the first term as shown in Fig. 3(a). A_m are undetermined coefficients. By applying the zero normal stress and imposed shear stress boundary conditions at $y = \pm b/2$, one can obtain the stress function ϕ_2 for this case as

$$\phi_2 = \sum_{m=1,3,5} \cos\left(\frac{m\pi x}{a}\right) \left[C_{2m} \sinh\left(\frac{m\pi y}{a}\right) + C_{3m} y \cosh\left(\frac{m\pi y}{a}\right) \right] \quad (8)$$

where C_{2m} and C_{3m} are given by

$$C_{2m} = \frac{a^2 b A_m \cosh\left(\frac{bm\pi}{2a}\right)}{bm^2 \pi^2 - am \pi \sinh\left(\frac{bm\pi}{a}\right)} \quad \text{and} \quad C_{3m} = -\frac{2a^2 A_m \sinh\left(\frac{bm\pi}{2a}\right)}{bm^2 \pi^2 - am \pi \sinh\left(\frac{bm\pi}{a}\right)} \quad (9)$$

This will impose a shear stress (Fig. 3(b)) at $x = \pm a/2$ as given by

$$\tau_2 = \pm \sum_{m=1,3,5..} \frac{m\pi}{a} \sin\left(\frac{m\pi}{2}\right) \left[\left(C_{2m} \frac{m\pi}{a} + C_{3m} \right) \cosh\left(\frac{m\pi y}{a}\right) + C_{3m} \frac{m\pi}{a} y \sinh\left(\frac{m\pi y}{a}\right) \right] \quad (10)$$

2.3 Building block 3

The third building block corresponds to imposed shear stresses at $x = \pm a/2$ as given by

$$\tau_{xy3} = \pm \sum_{n=2,4,6..} B_n \cos\left(\frac{n\pi y}{b}\right) \quad (11)$$

where B_n are undetermined coefficients and the first term is as shown in Fig. 4(a). The stress function for this building block is similar to that of the building block 1; the constants however, will take on different values when the condition of zero normal stress and applied shear stress are enforced along $x = \pm a/2$. The final solution is given by

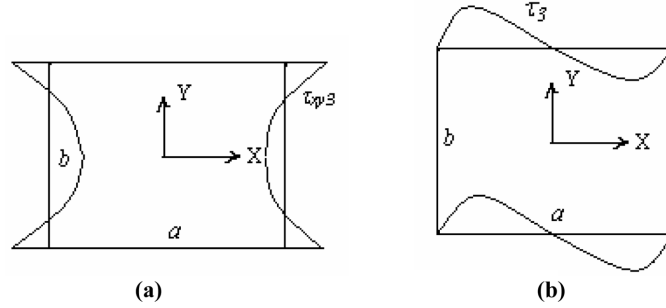


Fig. 4 (a) Building block 3, (b) The corresponding residual shear stress

$$\phi_3 = \sum_{n=2,4,6..} \sin\left(\frac{n\pi y}{b}\right) \left[C_{1n} \cosh\left(\frac{n\pi x}{b}\right) + C_{4n} x \sinh\left(\frac{n\pi x}{b}\right) \right] \quad (12)$$

where C_{1n} and C_{4n} are given by

$$C_{1n} = \frac{ab^2 B_n \sinh\left(\frac{an\pi}{2b}\right)}{an^2 \pi^2 + bn\pi \sinh\left(\frac{an\pi}{b}\right)} \quad \text{and} \quad C_{4n} = -\frac{2b^2 B_n \cosh\left(\frac{an\pi}{2b}\right)}{an^2 \pi^2 + bn\pi \sinh\left(\frac{an\pi}{b}\right)} \quad (13)$$

However, this will impose a shear stress (Fig. 4(b)) at $y = \pm b/2$ as given by

$$\tau_3 = - \sum_{n=2,4,6..} \frac{n\pi}{b} \cos\left(\frac{n\pi}{2}\right) \left[\left(C_{1n} \frac{n\pi}{b} + C_{4n} \right) \sinh\left(\frac{n\pi x}{b}\right) + C_{4n} \frac{n\pi}{b} x \cosh\left(\frac{n\pi x}{b}\right) \right] \quad (14)$$

2.4 Superposition

All the field equations and boundary conditions of this two-dimensional elasticity problem are satisfied by the above building blocks except those of zero shear stresses on the four edges of the plate. These conditions are now enforced on the net superposed solution to yield

$$\tau_1 + \tau_{yx2} + \tau_3 = 0 \quad \text{at} \quad y = \pm b/2 \quad (15)$$

$$\tau_2 + \tau_{yx3} = 0 \quad \text{at} \quad x = \pm a/2 \quad (16)$$

After expanding $\tau_1 + \tau_3$ into Fourier sine series and τ_2 into Fourier cosine series, one can reduce the above equations to a set of linear algebraic equations which yield the unknown coefficients A_n and B_m .

2.5 Results

The superposition of three stress functions is required so as to enforce the zero shear stress conditions at the edges of the plate. The convergence of the final superposed value of this stress towards zero with increase in the number of terms (A_n and B_m) considered in ϕ_2 and ϕ_3 is illustrated for one load case (Case 2) in Fig. 5; these results pertain to a square plate. This kind of study is

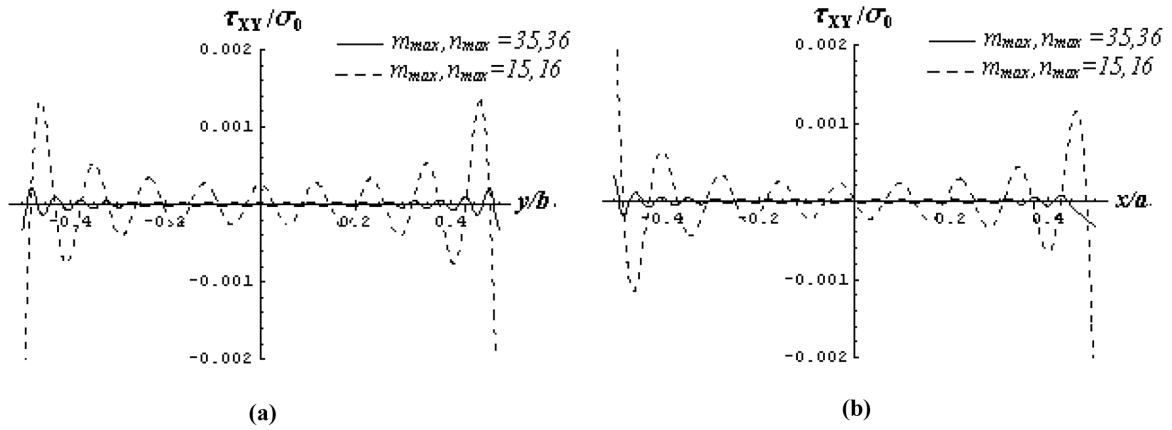


Fig. 5 Satisfaction of the zero shear condition at (a) $x = \pm a/2$, (b) $y = \pm b/2$

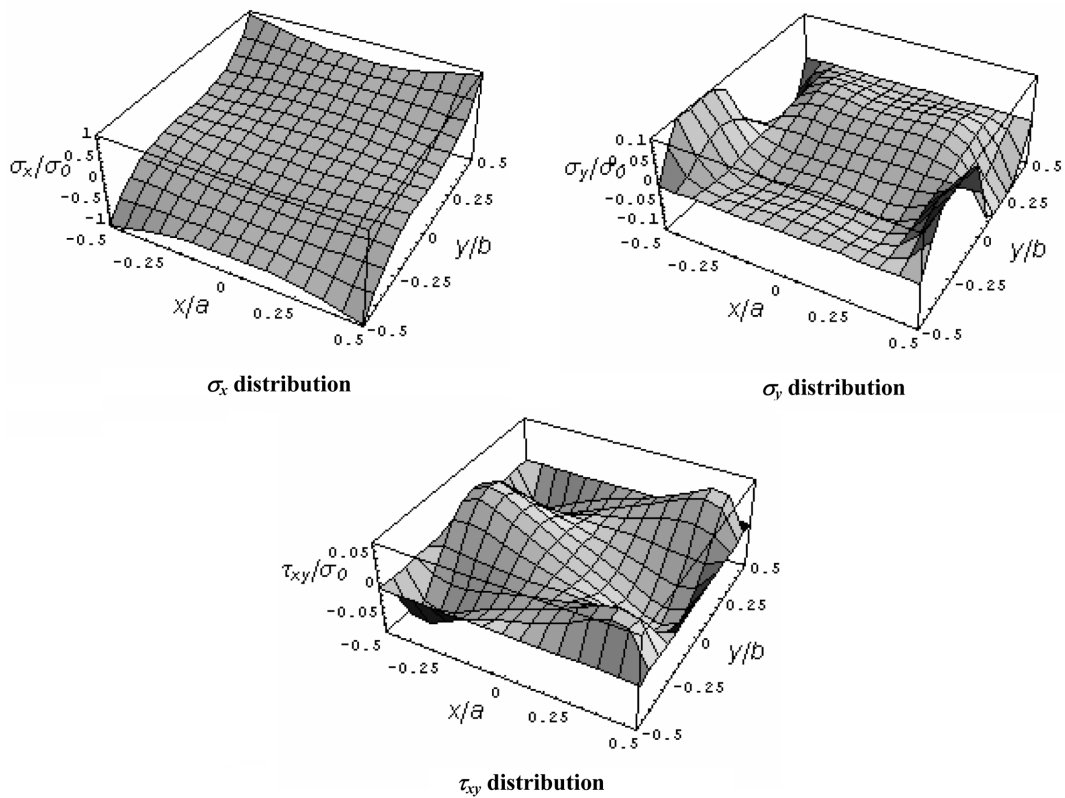


Fig. 6 In-plane stress field for load case 4 ($a/b = 1$)

carried out for each load case so as to ensure that the zero shear boundary condition is always numerically satisfied; with the other boundary conditions and the field equations already satisfied analytically, the present superposition method thus yields a rigorous solution for the plane stress problem.

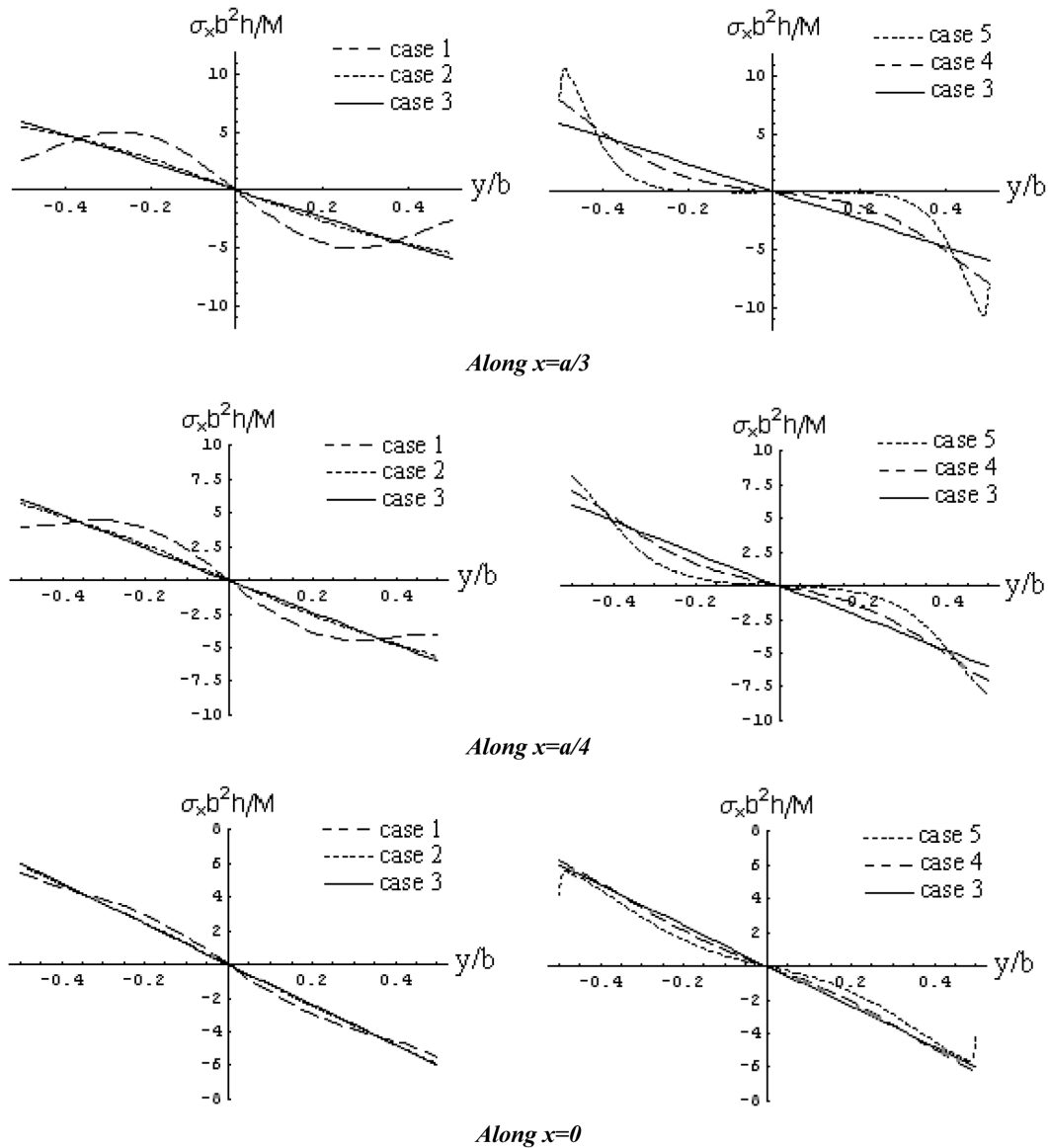
Fig. 7 Stress diffusion for different load cases ($a/b = 1$)

Fig. 6 shows a three-dimensional plot of the in-plane stresses for a square plate subjected to cubic load (load case 4). It can be seen from these figures that the stress field is characterized by non-zero σ_y and τ_{xy} and that these stresses, though small, are not insignificant as compared to σ_x . These additional non-zero stresses σ_y and τ_{xy} would naturally play a part in the buckling behaviour of the plate. This observation is true for all the other load cases except case 3 (i.e., the linear distribution).

Fig. 7 represents the comparison of σ_x stress distribution for the same total moment for the different load cases, with the patch size taken as $b/400$ for case 5. According to St. Venant's principle, all the load cases have a tendency to diffuse towards the linear one in the interior of the

plate. It is clear that this diffusion is quite rapid and the variation at the central section ($x = 0$) is nearly linear even for a square plate.

3. Stability analysis

The governing differential equation for thin plate buckling is

$$\nabla^4 w + \frac{h}{D} \left(\sigma_x \frac{\partial^2 w}{\partial x^2} + 2 \tau_{xy} \frac{\partial^2 w}{\partial x \partial y} + \sigma_y \frac{\partial^2 w}{\partial y^2} \right) = 0 \tag{17}$$

Owing to the complexity of this equation when each of the in-plane stresses is in series form, exact analytical solution is not possible. Therefore, the buckling solution is obtained by using the Galerkin method for the case of simply supported rectangular plates with the admissible functions

$$w = \sum_{m=1,2,3..} \sum_{n=1,2,3..} W_{mn} \sin \frac{m\pi}{a} \left(x + \frac{a}{2} \right) \sin \frac{n\pi}{b} \left(y + \frac{b}{2} \right) \tag{18}$$

which form a complete set, thus ensuring convergence to the exact solution with increase in the number of terms.

A verification of this methodology is possible by comparison with the exact solution of Kang and Leissa (2005) for the case of a linear variation of the edge load (Case 3); as pointed out earlier, their results were based on the rigorous solution of the buckling equation using Frobenius' series. A comparison of their results with the present ones for a set of aspect ratios is as shown in Table 1. As can be seen, the agreement is excellent with the first four significant digits being exactly the same.

The converged values of the critical bending moment corresponding to the chosen edge load distributions are presented in Table 2. For the case of localized load (case 5), the patch size is taken

Table 1 Validation study for the case of linear load (case 3)

| Method | Critical value of $\sigma_0 b^2/D$ | | |
|------------------------|------------------------------------|-----------|-------------|
| | $a/b = 2/3$ | $a/b = 1$ | $a/b = 3/2$ |
| Present | 235.7 | 252.0 | 238.0 |
| Kang and Leissa (2005) | 235.7 | 252.0 | 238.0 |

Table 2 Total critical bending moment (values of k in $M_{cr} = k\pi^2 D$) for different load cases

| Load cases | $a/b = 1.0$ | | $a/b = 2.0$ |
|---|----------------|-------|----------------|
| | Present method | NISA | Present method |
| 1. Full sine load | 3.119 | 3.047 | 3.402 |
| 2. Half sine load | 4.046 | 4.052 | 3.890 |
| 3. Linear load | 4.255 | 4.227 | 3.980 |
| 4. Cubic load | 5.069 | 5.035 | 4.324 |
| 5. Localised load (Patch size= $b/400$) | 5.915 | 5.871 | 4.661 |

to be $b/400$; it is found that the value of the critical bending moment varies by less than 1% when the patch size is varied between $b/50$ and $b/400$.

The results of Table 2 show that the critical bending moment increases when one moves from full sine load to the localized load in the order of case numbers – i.e., as the moment arm between the tensile and compressive force resultants increases. This has to be expected because the edges are supported and any moment applied predominantly at the centre of the plate has a greater tendency to cause lateral deformation and hence buckling. The actual results show that this effect changes the overall critical moment quite significantly for a square plate – with the values ranging from 0.73 to 1.39 times that for the case of linear stress distribution.

Table 2 also includes results found out using the finite element package NISA – *this is just to provide an idea of the errors involved in a straightforward use of a commercial package for the present type of problems*. The results presented are those based on a four-noded quadrilateral element with successive mesh refinement to ensure convergence. Though the finite element results are seen to agree well with those of the analytical solution, it is clear that exact coincidence cannot be achieved in spite of careful convergence studies.

As the aspect ratio (a/b) of the plate increases, the significance of the actual edge load distribution decreases. For instance, for $a/b = 2$, the different values as shown in Table 2 range from 0.85 to 1.17 times that for the case of linear stress distribution. For aspect ratios of 5 and more, the values for all the cases are found to be more or less the same.

Fig. 8 presents the qualitative picture of the mode shapes for a square plate. For all the load cases except the case of localized loads (Case 5), the mode shape for the square plate corresponds to zero nodal lines parallel to the x -axis and one nodal line parallel to the y -axis; for Case 5, the shape corresponds to zero nodal lines in both the directions. Thus, the number of nodal lines cannot be simply extrapolated from experience with the case of linear bending stress, but depends on the actual distribution considered.

The actual shapes of the buckled configuration are compared in Fig. 9 for the different cases for which the number of nodal lines is the same; each curve is normalized with respect to its peak value. It has to be noted that the variations in x and y directions are given by a summation of harmonic functions and are hence not simple one or two term functions. From Fig. 9, one can see that the buckled shapes are more or less the same for the four cases shown in the x -direction. This

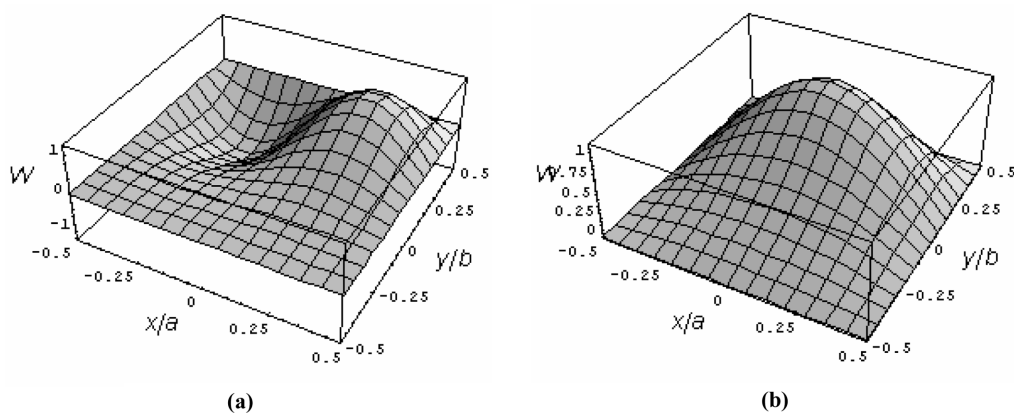


Fig. 8 Qualitative picture of the buckled shape for (a) Cases 1-4, (b) Case 5

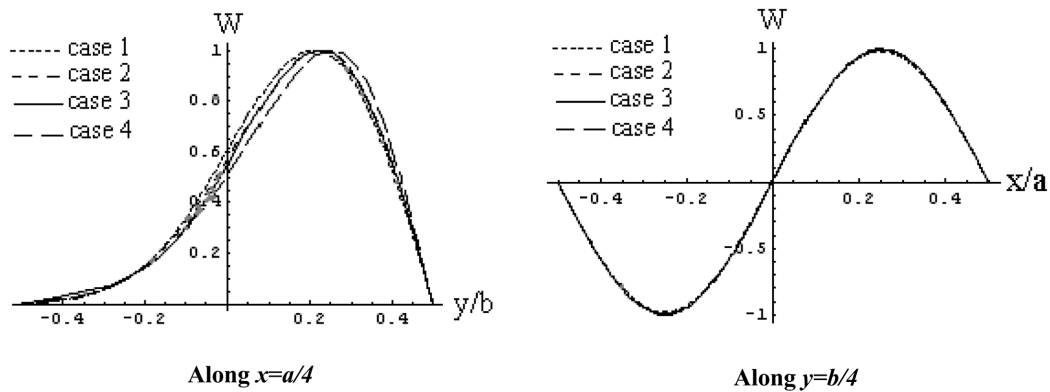


Fig. 9 Comparison of buckled shape for different cases

is also true in the y -direction, but for a slight shift of the peak value. It should be pointed out that the buckled shapes for cases 2 and 3 agree so well that they cannot be distinguished from the graphs.

4. Conclusions

Based on rigorous plane stress solutions, the buckling loads of plates under various bending stress distributions have been obtained. It has been shown that the actual distribution has a significant influence on the critical value of the total moment; further, the number of nodal lines of the buckled configuration can also be different. The primary purpose of the present investigation is to highlight the quantitative severity of different load distributions; however, the analytical results presented herein will also be of use in judging the accuracy of various approximate methods commonly used for such problems.

References

- Bedair, O.K. (1996), "Buckling behaviour of plates partially restrained against rotation under stress gradient", *Struct. Eng. Mech.*, **4**, 383-396.
- Benoy, M.B. (1969), "An energy solution for the buckling of rectangular plates under non-uniform in-plane loading", *Aeronaut. J.*, **73**, 974-977.
- Bert, C.W. and Devarakonda, K.K. (2003), "Buckling of rectangular plate subjected to nonlinearly distributed in-plane loading", *Int. J. Solids Struct.*, **40**, 4097-4106.
- Bulson, P.S. (1970), *The Stability of Flat Plates*, Chatto and Windus, London.
- Chen, X.L. and Liew, K.M. (2004), "Buckling of rectangular functionally graded material plates subjected to nonlinearly distributed in-plane edge loads", *Smart Mater. Struct.*, **13**, 1430-1437.
- Hu, H., Badir, A. and Abatan, A. (2003), "Buckling behavior of a graphite/epoxy composite plate under parabolic variation of axial loads", *Int. J. Mech. Sci.*, **45**, 1135-1147.
- Jana, Prasun and Bhaskar, K. (2004), "Buckling of rectangular plates under non-uniform compression using rigorous plane stress solutions", *Proc. of the Int. Conf. on Theoretical, Analytical, Computational and Experimental Mechanics*, IIT, Kharagpur, December.
- Jana, Prasun (2005), *Analytical Solutions for Buckling of Rectangular Plates due to Non-linearly Distributed*

- Uniaxial and Biaxial Loads*, Master's thesis, IIT, Madras.
- Kang, J.H. and Liessa, A.W. (2005), "Exact solutions for the buckling of rectangular plates having linearly varying in-plane loading on two opposite simply supported edges", *Int. J. Solids Struct.*, **42**, 4220-4238.
- Liew, K.M. and Chen, X.L. (2004), "Buckling of rectangular Mindlin plates subjected to partial in-plane edge loads using the radial point interpolation method", *Int. J. Solids Struct.*, **41**, 1677-1695.
- Leissa, A.W. and Ayoub, E.F. (1988), "Vibration and buckling of a simply supported rectangular plate subjected to a pair of in-plane concentrated forces", *J. Sound Vib.*, **127**, 155-171.
- Leissa, A.W. and Kang, J.H. (2002), "Exact solutions for vibration and buckling of an SS-C-SS-C rectangular plate loaded by linearly varying in-plane stresses", *Int. J. Mech. Sci.*, **44**, 1925-1945.
- Little, R.W. (1973), *Elasticity*, Prentice Hall, Englewood Cliffs, NJ.
- Srivastava, A.K.L., Datta, P.K. and Sheikh, A.H. (2003), "Buckling and vibration of stiffened plates subjected to partial edge loading", *Int. J. Mech. Sci.*, **45**, 73-93.
- Timoshenko, S.P. (1910), "Stabilitat einer rechteckigen platte, die durch einzelne krafte gedreht wird", *ZAMP*, **58**, 357-360.
- Timoshenko, S.P. and Gere, J.M. (1961), *Theory of Elastic Stability*, McGraw-Hill, New York.